Elucidation of the Structure of a Thiol Functionalized Cu-tmpa Complex Anchored to Gold via a Self-Assembled Monolayer

Smits, N.W.G.; Boer, D. den; Wu, L.; Hofmann, J.P.; Hetterscheid, D.G.H.

Inorganic Chemistry
Cite This: Inorg. Chem. 2019, 58, 13007−13019
Article
pubs.acs.org/IC

Elucidation of the Structure of a Thiol Functionalized Cu-tmpa Complex Anchored to Gold via a Self-Assembled Monolayer

Nicole W. G. Smits,[†] Daan den Boer,[†] Longfei Wu,[‡,§] Jan P. Hofmann,[‡] and Dennis G. H. Hetterscheid*[,†]

[†]Leiden Institute of Chemistry, Leiden University, P.O. Box 9502, 2300 RA Leiden, The Netherlands

[‡]Laboratory for Inorganic Materials and Catalysis, Department of Chemical Engineering and Chemistry, Eindhoven University of Technology, P.O. Box 513, 5600 MB Eindhoven, The Netherlands

Supporting Information

ABSTRACT: The structure of the copper complex of the 6-((1-butanethiol)oxy)-tris(2-pyridylmethyl)amine ligand (Cu-tmpa-O$(CH_2)_4$SH) anchored to a gold surface has been investigated. To enable covalent attachment of the complex to the gold surface, a heteromolecular self-assembled monolayer (SAM) of butanethiol and a thiol-substituted tmpa ligand was used. Subsequent formation of the immobilized copper complex by cyclic voltammetry in the presence of Cu$(OTf)_2$ resulted in the formation of the anchored Cu-tmpa-O$(CH_2)_4$SH system which, according to scanning electron microscopy and X-ray diffraction, did not contain any accumulated copper nanoparticles or crystalline copper material. Electrochemical investigation of the heterogenized system barely showed any redox activity and lacked the typical $Cu^{II/I}$ redox couple in contrast to the homogeneous complex in solution. The difference between the heterogenized system and the homogeneous complex was confirmed by X-ray photoelectron spectroscopy; the XPS spectrum did not show any satellite features of a Cu^{II} species but instead showed the presence of a Cu^{I} ion in a ∼2:3 ratio to nitrogen and a ∼2:7 ratio to sulfur. The +I oxidation state of the copper species was confirmed by the edge position in the X-ray absorption near-edge structure (XANES) region of the X-ray absorption spectrum. These results show that upon immobilization of Cu-tmpa-O$(CH_2)_4$SH, the resulting structure is not identical to the homogeneous Cu^{II}-tmpa complex. Upon anchoring, a novel Cu^{I} species is formed instead. This illustrates the importance of a thorough characterization of heterogenized molecular systems before drawing any conclusions regarding the structure−function relationships.

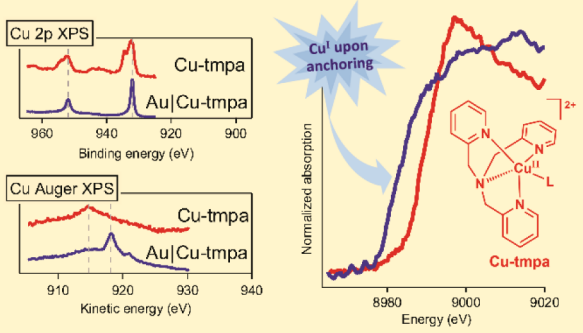

INTRODUCTION

The immobilization of transition metal complexes onto surfaces is an important technique which is used for a wide variety of applications.[1−19] Examples involve chemical sensing,[1−4] light harvesting,[5−7] drug delivery,[8,9] and *in situ* characterization of catalytic species.[10,11] Even though immobilized transition metal sites with a very high level of complexity have been reported, detailed characterization of the structure of a relatively small amount of anchored complex is a very challenging process. Often it is simply assumed that the structure of the heterogenized complex is identical to the homogeneous complex in solution. This is off course not necessarily the case. Particularly when a metal surface is being used as the support ambiguity regarding the precise oxidation state of the immobilized coordination site is to be expected due to for example valence tautomerism involving the support.

An excellent method for the immobilization of coordination complexes to metal substrates in a well-defined manner involves self-assembled monolayers (SAMs). Such a SAM consists of a molecular assembly which forms spontaneously on a surface by chemisorption. In particular the formation of SAMs based on thiol-substituted alkyls on gold surfaces has historically been studied in great detail. Upon immersion of the gold substrate into a solution of the thiol compound of interest, the thiol readily attaches to the gold surface with the formation of a relatively strong gold thiolate bond. This typically results in the formation of a well-defined SAM with relatively little defects on Au(111).[20]

Characterization of an immobilized coordination complex has been performed in case the complex as a whole was anchored.[7,21,22] However, little reports to date have confidently shown that both the structure and oxidation state of a more dynamic coordination site stay intact upon covalent anchoring to a metal substrate.

We have investigated and elucidated the structure of a thiol functionalized copper complex of the tris(2-pyridylmethyl)-amine ligand (Cu-tmpa) which was anchored to a gold electrode surface with the aid of a heteromolecular SAM. Cu-tmpa is a well-known homogeneous catalyst for atom transfer

Received: June 28, 2019
Published: September 24, 2019

radical polymerization (ATRP)[23] and for the oxygen reduction reaction (ORR).[24−28] The catalyst has also been studied heterogeneously by physisorption onto a carbon support and consecutive dropcasting onto a glassy carbon electrode.[29−31]

Upon anchoring the Cu complex to a gold electrode via a SAM, we show that the structure of the anchored Cu complex of interest deviates substantially from the structure of homogeneous Cu^{II}-tmpa itself. Rather than formation of a typical Cu^{II} complex at the electrode surface, X-ray photoelectron spectroscopy (XPS) and X-ray absorption spectroscopy (XAS) point toward a Cu^{I} coordination polymer with an unexpected high copper content.

EXPERIMENTAL SECTION

Materials and Methods. $[Cu(tmpa)(MeCN)](OTf)_2$ was afforded as reported.[28] 4-((^{t}Butyldimethylsilyl)oxy)butan-1-ol was obtained from Santa Cruz Biotechnology and used as received. All other chemicals and solvents were purchased from Merck or VWR and were used as received as well. Deoxygenated and anhydrous solvents were obtained from a PureSolv PS-MD-5 solvent dispenser (Innovative Technology). Column chromatography was performed on alumina (Al_2O_3, activated, basic, Brockmann I, 58 Å pore size, pH 9.5 ± 0.5) . Thin layer chromatography (TLC) was performed using TLC plates from Machery-Nagel (Alugram Aloz, Al_2O_3, with F_{254} indicator on aluminum backing, pH 9). Compounds were visualized on TLC plates by UV detection at 254 nm. ^{1}H, COSY, ^{13}C APT, HSQC, and HMBC NMR spectra were recorded on a Bruker 400 MHz (100.6 MHz for ^{13}C) NMR spectrometer using the residual solvent as internal standard. Mass spectra were obtained by high resolution mass spectrometry (HRMS) using a TOF Synapt G2-Si mass spectrometer equipped with an electrospray ionization source in positive ion mode with leu-enkephalin (m/z = 556.2771) as an internal lock mass. TLC/mass spectrometry (TLC/MS) analysis was performed on an Advion Plate Express TLC Plate Reader connected to an Advion expression^L CMS mass spectrometer.

*Synthesis of 6-Bromo-tris(2-pyridylmethyl)amine (**1**).* A solution of 6-bromo-2-pyridinecarboxaldehyde (2.00 g, 10.7 mmol) and di(2-picolyl)amine (2.0 mL, 11.1 mmol) in deoxygenated and anhydrous THF (75 mL) under a N_2 atmosphere containing 3 Å molecular sieves was stirred at room temperature (r.t.) for 1.5 h before the addition of sodium triacetoxyborohydride (3.47 g, 16.4 mmol). After stirring at r.t. overnight, the mixture was filtered, concentrated under reduced pressure, and redissolved in EtOAc. The organic solution was washed with saturated aqueous $NaHCO_3$ (3 × 40 mL). After extraction of the aqueous layer with EtOAc (2 × 30 mL), the combined organic layers were dried over $MgSO_4$. Filtration and solvent removal under reduced pressure afforded the product as a dark yellow solid (3.63 g, 9.8 mmol, 92%). R_f 0.30 (Al_2O_3 pH 9, 1:3 EtOAc/petroleum ether). ^{1}H NMR (400 MHz, $CDCl_3$, 293 K): δ 8.52 (ddd, ^3J(H,H) = 4.9, ^4J(H,H) = 1.8, ^5J(H,H) = 0.9 Hz, 2H, *o*-Py*H*), 7.64 (td, ^3J(H,H) = 7.7, ^4J(H,H) = 1.8 Hz, 2H, *p*-Py*H*), 7.60−7.52 (m, 3H, Py-NCC*H* and *o*-BrPy-NCCH$_2$C*H*), 7.49 (t, ^3J(H,H) = 7.7 Hz, 1H, *p*-(*o*-BrPy)*H*), 7.31 (dd, ^3J(H,H) = 7.7, ^4J(H,H) = 0.9 Hz, 1H, *o*-BrPy-NCBrC*H*), 7.13 (ddd, ^3J(H,H) = 7.5, 4.9, ^4J(H,H) = 1.3 Hz, 2H, Py-NCHC*H*), 3.87 (s, 4H, *o*-PyCH_2), 3.86 (s, 2H, *o*-(*o*-BrPy)CH_2) ppm. ^{13}C NMR (100.6 MHz, $CDCl_3$, 293 K): δ 161.33 (*o*-(*o*-BrPy)CCH_2), 159.14 (*o*-PyCCH_2), 149.27 (*o*-PyCH), 141.38 (*o*-(*o*-BrPy)CBr), 138.89 (*p*-(*o*-BrPy)CH), 136.56 (Py-NCHCH), 126.33 (*o*-BrPy-NCBrCH), 123.10 (Py-NCCH), 122.20 (*p*-PyCH), 121.69 (*o*-BrPy-NCCH$_2$CH), 60.24 (*o*-PyCH_2), 59.53 (*o*-(*o*-BrPy)CH_2) ppm. HRMS (ESI): 369.0720; calc. $[M+H^+]^+$: 369.0709.

*Synthesis of 6-((^{t}Butyldimethylsilyl)oxy)butoxy-tris(2-pyridylmethyl)amine (**2**).* Sodium hydride (60 wt % dispersion in mineral oil, 0.88 g, 22.1 mmol) was added to a stirring solution of 4-((^{t}butyldimethylsilyl)oxy)-1-butanol (1.24 mL, 5.4 mmol) in deoxygenated and anhydrous THF (60 mL) under a N_2 atmosphere at 0 °C. After several minutes, **1** (2.00 g, 5.4 mmol) was added. Overnight refluxing was followed by cooling to r.t. and quenching of the remaining NaH with MeOH. The mixture was concentrated under reduced pressure, and the concentrated crude was redissolved in EtOAc (100 mL). The organic solution was washed with H_2O (150 mL) and brine (140 mL), dried over $MgSO_4$, filtered, and concentrated under reduced pressure to afford the product as a brown oil (2.77 g) which was used without further purification. R_f 0.65 (Al_2O_3 pH 9, EtOAc). ^{1}H NMR (400 MHz, $CDCl_3$, 293 K): δ 8.51 (dt, ^3J(H,H) = 4.9, ^4J(H,H) and ^5J(H,H) = 1.4 Hz, 2H, *o*-Py*H*), 7.69−7.57 (m, 4H, *p*-Py*H* and Py-NCC*H*), 7.51 (dd, ^3J(H,H) = 8.2, 7.2 Hz, 1H, *p*-(*o*-OPy)*H*), 7.18−7.07 (m, 2H, Py-NCHC*H*), 7.06 (d, ^3J(H,H) = 7.2 Hz, 1H, *o*-OPy-NCCH$_2$C*H*), 6.56 (d, ^3J(H,H) = 8.2 Hz, 1H, *o*-OPy-NCOC*H*), 4.30 (t, ^3J(H,H) = 6.6 Hz, 2H, *o*-(*o*-OPy)OCH_2), 3.90 (s, 4H, *o*-PyCH_2), 3.75 (s, 2H, *o*-OPy-CH_2), 3.66 (t, ^3J(H,H) = 6.5 Hz, 2H, *o*-(*o*-OPy)OCH$_2$CH$_2$CH$_2$CH_2), 1.88−1.76 (m, 2H, *o*-(*o*-OPy)OCH$_2$CH$_2$CH_2), 1.74−1.60 (m, 2H, *o*-(*o*-OPy)-OCH$_2$CH_2), 0.88 (s, 9H, Si(CH$_3$)$_2$C(CH_3)$_3$), 0.04 (s, 6H, Si(CH_3)$_2$) ppm. ^{13}C NMR (100.6 MHz, $CDCl_3$, 293 K): δ 163.60 (*o*-(*o*-OPy)CO)), 159.95 (*o*-PyCCH_2), 157.01 (*o*-(*o*-OPy)CCH_2), 149.17 (*o*-PyCH), 138.90 (*p*-(*o*-OPy)CH), 136.53 (Py-NCHCH or *p*-PyCH), 122.82 (Py-NCCH), 122.03 (Py-NCHCH or *p*-PyCH), 115.31 (*o*-OPy-NCCH$_2$CH), 108.86 (*o*-OPy-NCOCH), 65.81 (*o*-(*o*-OPy)-OCH$_2$), 63.04 (*o*-(*o*-OPy)OCH$_2$CH$_2$CH$_2$CH$_2$), 60.33 (*o*-PyCH_2), 59.80 (*o*-(*o*-OPy)CH_2), 29.62 (*o*-(*o*-OPy)OCH$_2$CH_2), 26.10 (Si-(CH$_3$)$_2$C(CH_3)$_3$), 25.79 (*o*-(*o*-OPy)OCH$_2$CH$_2$CH_2), 18.48 (Si-(CH$_3$)$_2$C(CH$_3$)$_3$), − 5.13 (Si(CH_3)$_2$) ppm. HRMS (ESI): 493.2993; calc. $[M+H^+]^+$: 493.2993.

*Synthesis of 6-((1-Butanol)oxy)-tris(2-pyridylmethyl)amine (**3**).* Tetra-^{n}butylammonium fluoride (1 M in THF, 6.0 mL, 6.0 mmol) was added dropwise to a stirring solution of **2** (1.47 g, 2.98 mmol) in deoxygenated and anhydrous THF (40 mL) under a N_2 atmosphere at 0 °C. After stirring the mixture at 0 °C for 6 h, it was warmed to r.t. and concentrated under reduced pressure. Column chromatography (Al_2O_3 pH 9.5 ± 0.5, gradient: 10% petroleum ether in EtOAc to 3% MeOH in EtOAc) afforded the product as a light yellow oil (0.74 g, 1.94 mmol, 68% over two steps from compound **1** to compound **3**). R_f 0.30 (Al_2O_3 pH 9, 3% MeOH in EtOAc). ^{1}H NMR (400 MHz, $CDCl_3$, 283 K): δ 8.50 (dt, ^3J(H,H) = 4.8, ^4J(H,H) and ^5J(H,H) = 1.3 Hz, 2H, *o*-Py*H*), 7.70−7.60 (m, 4H, *p*-Py*H* and Py-NCCH$_2$C*H*), 7.50 (dd, ^3J(H,H) = 8.2, 7.2 Hz, 1H, *p*-(*o*-OPy)*H*), 7.13 (m, 2H, Py-NCHC*H*), 6.97 (d, ^3J(H,H) = 7.2 Hz, 1H, *o*-OPy-NCCH$_2$C*H*), 6.57 (d, ^3J(H,H) = 8.2 Hz, 1H, *o*-OPy-NCOC*H*), 4.37 (t, ^3J(H,H) = 6.7 Hz, 2H, CH_2CH$_2$CH$_2$CH$_2$OH), 3.94 (s, 4H, *o*-PyCH_2), 3.79 (s, 2H, *o*-(*o*-OPy)CH_2), 3.72 (t, ^3J(H,H) = 6.3 Hz, 2H, CH_2OH), 2.95 (s, 1H, O*H*), 1.88 (m, 2H, CH_2CH$_2$CH$_2$OH), 1.72 (m, 2H, CH_2CH$_2$OH) ppm. ^{13}C NMR (100.6 MHz, $CDCl_3$, 293 Hz): δ 163.38 (*o*-(*o*-OPy)CO), 159.94 (*o*-PyCCH_2), 156.47 (*o*-(*o*-OPy)CCH_2), 149.07 (*o*-PyCH), 138.93 (*p*-(*o*-OPy)*H*), 136.63 (p-PyCH), 122.75 (Py-NCCH), 122.04 (Py-NCHCH), 115.77 (*o*-OPy-NCCH$_2$CH), 109.13 (*o*-OPy-NCOCH), 65.51 (CH$_2$CH$_2$CH$_2$CH$_2$OH), 62.40 (CH_2OH), 60.08 (*o*-PyCH_2), 59.44 (*o*-(*o*-OPy)CH_2), 29.40 (CH_2CH$_2$OH), 25.80 (CH$_2$CH_2CH$_2$OH) ppm. HRMS (ESI): 379.2133; calc. $[M+H^+]^+$: 379.2129.

*Synthesis of 6-(4-Chlorobutoxy)-tris(2-pyridylmethyl)amine (**4**).* A solution of $SOCl_2$ (55 μL, 0.75 mmol) in $CHCl_3$ (1 mL) was added dropwise to a stirring solution of **3** (192 mg, 0.51 mmol) in $CHCl_3$ (2 mL) at 0 °C. The mixture was stirred at r.t. overnight and quenched by the addition of H_2O. Saturated aqueous $NaHCO_3$ was added until the pH of the solution was around 9. The mixture was extracted four times with CH_2Cl_2, and the combined organic layers were washed with brine. The organic phase was dried over $MgSO_4$, filtered, and concentrated under reduced pressure to obtain the product as a dark brown oil (162 mg, 0.41 mmol, 80%). R_f 0.80 (Al_2O_3 pH 9, 3% MeOH in EtOAc). ^{1}H NMR (400 MHz, $CDCl_3$, 293 K): δ 8.51 (dt, ^3J(H,H) = 4.8, ^4J(H,H) and ^5J(H,H) = 1.3 Hz, 2H, *o*-Py*H*), 7.68−7.60 (m, 4H, *p*-Py*H* and Py-NCC*H*), 7.52 (dd, ^3J(H,H) = 8.2, 7.3 Hz, 1H, *p*-(*o*-OPy)*H*), 7.17−7.10 (m, 2H, Py-NCHC*H*), 7.05 (d, ^3J(H,H) = 7.3 Hz, 1H, *o*-OPy-NCCH$_2$C*H*), 6.56 (d, ^3J(H,H) = 8.2 Hz, 1H, *o*-OPy-NCOC*H*), 4.32 (t, ^3J(H,H) = 6.0 Hz, 2H, CH_2CH$_2$CH$_2$CH$_2$Cl), 3.92 (s, 4H, *o*-PyCH_2), 3.77 (s, 2H, *o*-(*o*-OPy)CH_2), 3.60 (t, ^3J(H,H) = 6.3 Hz, 2H, CH_2Cl), 2.00−1.84 (m,

DOI: 10.1021/acs.inorgchem.9b01921
Inorg. Chem. 2019, 58, 13007−13019

4H, $CH_2CH_2CH_2Cl$ and CH_2CH_2Cl) ppm. ^{13}C NMR (100.6 MHz, $CDCl_3$, 293 K): δ 163.36 (*o*-(*o*-OPy)CO), 159.72 (*o*-PyCCH$_2$), 156.80 (*o*-(*o*-OPy)CCH$_2$), 149.15 (*o*-PyCH), 139.00 (*p*-(*o*-OPy)CH), 136.56 (*p*-PyCH), 122.82 (Py-NCCH), 122.08 (Py-NCHCH), 115.56 (*o*-OPy-NCCH$_2$CH), 108.96 (*o*-OPy-NCOCH), 64.87 ($CH_2CH_2CH_2CH_2Cl$), 60.25 (*o*-PyCH$_2$), 59.69 (*o*-(*o*-OPy)CH$_2$), 44.98 (CH_2Cl), 29.52 ($CH_2CH_2CH_2Cl$ or CH_2CH_2Cl), 26.64 ($CH_2CH_2CH_2Cl$ or CH_2CH_2Cl) ppm. HRMS (ESI): 397.1793; calc. $[M+H^+]^+$: 397.1790.

*Synthesis of 6-((1-Butanethiol)oxy)-tris(2-pyridylmethyl)amine (**5**).* After refluxing a brown solution of **4** (102 mg, 0.26 mmol), KI (6.2 mg, 0.037 mmol), and thiourea (102 mg, 1.34 mmol) in EtOH (4 mL) for 2 days, TLC/MS analysis showed complete conversion of the starting material to the intermediate isothiouronium salt. $NaHCO_3$ (54 mg, 0.64 mmol) was added to the mixture, and TLC/MS analysis showed complete conversion of the isothiouronium salt after an overnight reflux. Cooling to r.t. was followed by addition of CH_2Cl_2 (20 mL) and saturated aqueous $NaHCO_3$ (20 mL). Collection of the organic layer was followed by extraction of the aqueous phase with CH_2Cl_2 (2 × 20 mL). The combined organic layers were dried over Na_2SO_4, filtered, and concentrated under reduced pressure. The resulting brown oil was purified by column chromatography (Al_2O_3 pH 9, 100% CH_2Cl_2 followed by 0.25% MeOH in CH_2Cl_2) to afford the desired thiol ligand as a yellow oil (27.1 mg, 69 μmol, 27%). R_f 0.40 (Al_2O_3 pH 9, 100% EtOAc). ^1H NMR (300 MHz, $CDCl_3$, 293 K): δ 8.51 (dt, ^3J(H,H) = 4.8, ^4J(H,H) and ^5J(H,H) = 1.3 Hz, 2H, *o*-Py*H*), 7.66−7.61 (m, 4H, *p*-Py*H* and Py-NCHC*H*), 7.54−7.45 (m, 1H, *p*-(*o*-OPy)*H*), 7.17−7.08 (m, 2H, Py-NCC*H*), 7.04 (d, ^3J(H,H) = 7.3 Hz, 1H, *o*-OPy-NCCH$_2$C*H*), 6.56 (d, ^3J(H,H) = 8.2 Hz, 1H, *o*-OPy-NCOC*H*), 4.36−4.26 (m, 2H, $CH_2CH_2CH_2CH_2SH$), 3.90 (s, 4H, *o*-PyCH_2), 3.75 (s, 2H, *o*-(*o*-OPy)CH_2), 3.05−2.85 (m, 2H, CH_2CH_2SH), 2.73 (t, ^3J(H,H) = 6.9 Hz, 1H, S*H*), 1.96−1.80 (m, 4H, $CH_2CH_2CH_2SH$ and CH_2SH) ppm. ^{13}C NMR (75.4 MHz, $CDCl_3$, 293 K): δ 163.42 (*o*-(*o*-OPy)CO), 159.84 (*o*-PyCCH$_2$), 156.92 (*o*-(*o*-OPy)CCH$_2$), 149.15 (*o*-PyCH), 138.94 (*p*-(*o*-OPy)CH), 136.52 (Py-NCHCH), 122.83 (p-PyCH), 122.04 (Py-NCCH), 115.50 (CH, *o*-OPy-NCCH$_2$CH), 108.96 (*o*-OPy-NCOCH), 65.19 ($CH_2CH_2CH_2CH_2SH$), 60.31 (*o*-PyCH$_2$), 59.73 (*o*-(*o*-OPy)CH$_2$), 38.58 (CH_2CH_2SH), 28.07 (CH_2SH), 25.63 ($CH_2CH_2CH_2SH$) ppm. HRMS (ESI): 787.3572; calc. $[disulfide+H^+]^+$ 787.3571; 394.1830; calc. $[disulfide+2H^+]^{2+}$ 394.1822.

Electrochemical Experiments. Milli-Q Ultrapure grade water (>18.2 MΩ cm resistivity) was used for all electrochemical experiments and for the preparation of aqueous solutions. All chemicals used for the preparation of the aqueous electrolyte and the buffer solutions were purchased from commercial sources and used without further purification. The 100 mM 4-(2-hydroxyethyl)-piperazine-1-ethanesulfonic acid (HEPES) buffer solution in 75 mM Na_2SO_4 electrolyte was prepared from HEPES (≥99.5% purity, Merck), and Na_2SO_4 (Suprapur, 99.99% purity, Merck) and was adjusted to pH 7 using NaOH·H_2O (TraceSELECT, ≥ 99.9995% purity, Fluka). The 0.3 mM $Cu(OTf)_2$ solution in 100 mM pH 7 HEPES buffer was prepared from $Cu(OTf)_2$ (≥99% purity, Alfa Aesar), and the 100 mM pH 7 HEPES buffer solution in 75 mM Na_2SO_4 electrolyte. Polishing pads and alumina micropolish suspensions (1.0, 0.3, and 0.05 μm) were obtained from Buehler. pH measurements were performed on a Hanna Instruments HI 4222 pH meter which was calibrated using IUPAC standard buffers.

All glassware used for electrochemical measurements was routinely cleaned of any organic contamination by overnight immersion in a 0.5 M aqueous H_2SO_4 solution containing 1 g/L $KMnO_4$. The glassware was afterward immersed in Milli-Q water containing a few droplets of concentrated H_2SO_4 and H_2O_2 for 30 min. The glassware was then cleaned by 3-fold boiling in Milli-Q water. Prior to each experiment, the glassware was boiled once in Milli-Q water, and rinsed 3-fold with Milli-Q water. All electrochemical measurements were performed in custom-made single-compartment 10 mL glass cells using a three-electrode configuration with an Autolab PGSTAT 12, 204, or 128N potentiostat operated by NOVA software.

All electrochemical experiments were carried out under either an argon (Linde, Ar 5.0) or an oxygen (Linde, O_2 5.0) atmosphere, and the gas was bubbled through the electrolyte for at least 15 min prior to the experiment. The atmosphere was maintained during the experiments by flowing 1 atm of the gas over the electrolyte. The counter electrode was a large surface area coiled gold wire (99.9% purity) that was flame annealed and rinsed with Milli-Q water prior to use. The reference electrode was a platinum mesh in H_2 (Linde, H_2 5.0) saturated 100 mM pH 7 HEPES buffer solution in 75 mM Na_2SO_4 electrolyte. The cell and reference electrode were connected via a Luggin capillary. The gold working electrode (WE) consisted of a flat disk with a geometric surface area of 0.031 cm^2 embedded in a polyether ether ketone (PEEK) holder and was purchased from Metrohm. Prior to use, the gold WE was manually polished using a polishing pad and 1.0 μm, 0.3 μm, and 0.05 μm alumina micropolish, consecutively, for 90 s each and sonicated once in Milli-Q water for 15 min. The WE was subsequently polished electrochemically by cyclic voltammetry (CV) between 0 and 1.75 V vs RHE for 200 cycles at a 1 V/s scan rate in a 0.1 M $HClO_4$ solution under an argon atmosphere. The effective surface area of the WE was used to convert measured currents to current densities. This area was obtained via the total charge of the reduction of gold oxide to polycrystalline gold during the last cycle of the electrochemical polish of the WE, and the reference charge of polycrystalline Au.[32] The gold thiolate bond proved to be extremely labile in the presence of both air and light, a phenomenon previously described in the literature.[33] Therefore, all measurements performed under an oxygen atmosphere involving a gold electrode modified with a SAM were carried out in the dark. Transportation and storage of the modified gold electrodes between consecutive measurements were performed in the dark and under a N_2 atmosphere, respectively.

Electrode Modifications. As previously described in the literature, the gold thiolate bond is photooxidatively labile which leads to oxidation of the thiolate to a sulfonate in the presence of UV light.[33] The SAMs formed during this study proved to be extremely labile in the presence of both air and light. All modification steps described below were therefore carried out under an inert atmosphere (argon for CV and N_2 for all other steps) and especially when the system was exposed to dioxygen or air, were performed rigorously in the dark. All wash steps described below were performed by dipping instead of rinsing, since the gold thiolate bond proved to be labile when washing was performed with a squeeze bottle.

Au|mixed SAM. The heteromolecular SAM of interest was formed by immersion of a polished gold WE in a 2 mM solution of **5** and 1-butanethiol (98% purity, Acros) in a 1:1 ratio in ethanol (≥99.8% purity, Merck) for 19−20 h. To ensure removal of any unanchored hydrophobic thiol compound from the gold surface, the modified WE was washed by a 5 s dip in ethanol in the dark after the initial anchoring of the thiol compounds. A subsequent 5 s dip in Milli-Q water in the dark ensured removal of the ethanol droplet which was left behind during the ethanol wash and afforded modified WE **Au|mixed SAM**.

^{CV}Au|mixed SAM|Cu. After anchoring of the heteromolecular SAM to the gold surface, copper was introduced by cyclic voltammetry (CV) of modified WE **Au|mixed SAM** in a 0.3 mM $Cu(OTf)_2$ solution in 100 mM pH 7 HEPES buffer under an argon atmosphere. During the voltammetry, the potential was cycled five times between 0.7 and 0.0 V vs RHE at 100 mV s^{-1}. A subsequent 5 s dip in Milli-Q water in the dark to ensure removal of any unanchored species afforded modified WE **^{CV}Au|mixed SAM|Cu**.

^{EDTA}Au|mixed SAM|Cu. To ensure removal of all noncoordinated excess copper species after the introduction of copper, modified WE **^{CV}Au|mixed SAM|Cu** was immersed into a 10 mM solution of the chelating agent disodium ethylenediaminetetraacetate dihydrate (EDTA; Merck) in Milli-Q water for 30 min. Removal of any unanchored species was performed by a subsequent 5 s dip in Milli-Q water in the dark and afforded modified WE **^{EDTA}Au|mixed SAM|Cu**.

^{ORR}Au|mixed SAM|Cu. The oxygen reduction reaction (ORR) catalysis of modified WE **^{EDTA}Au|mixed SAM|Cu** was performed in 100 mM pH 7 HEPES buffer under an oxygen atmosphere by CV

DOI: 10.1021/acs.inorgchem.9b01921
Inorg. Chem. 2019, 58, 13007−13019

Scheme 1. Synthetic Pathway toward the Thiol Ligand of Interest[a]

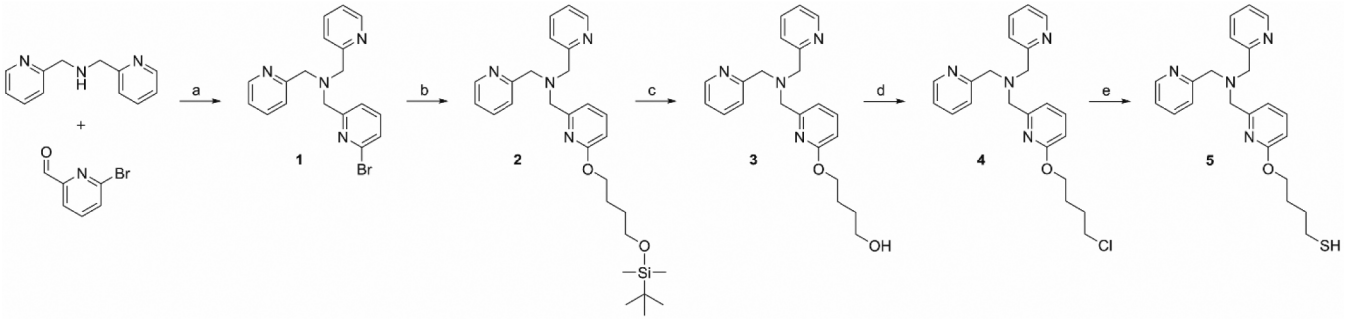

[a]Reagents and conditions: (a) $NaBH(OAc)_3$, THF, 3 Å molecular sieves, N_2 atm., r.t., overnight, 92%; (b) 4-((ᵗbutyldimethylsilyl)oxy)butan-1-ol, NaH, THF, N_2 atm., reflux, overnight; (c) TBAF, THF, 0 °C, 6 h, 68% over 2 steps; (d) $SOCl_2$, $CHCl_3$, r.t., overnight, 80%; (e) 1. thiourea, KI, EtOH, reflux, 2 days, 2. $NaHCO_3$, EtOH, reflux, overnight, 27%.

between 0.7 and 0.0 V vs RHE for 5 cycles in the dark. A subsequent 5 s dip in Milli-Q water in the dark to ensure removal of any unanchored species afforded modified WE ^{ORR}**Au|mixed SAM|Cu**.

Au|Butanethiol. The homomolecular reference SAM was formed by immersion of a polished gold WE in a 1 mM solution of 1-butanethiol in ethanol for 19−20 h. To ensure removal of any unanchored hydrophobic butanethiol from the gold electrode, the modified WE was washed by a 5 s dip in ethanol in the dark after the initial anchoring of the butanethiol. A subsequent 5 s dip in Milli-Q water in the dark ensured removal of the ethanol droplet which was left behind during the ethanol wash and afforded modified WE **Au|butanethiol**.

^{CV}Au|Butanethiol|Cu. After anchoring of the homomolecular reference SAM to the gold surface, copper was introduced by cyclic voltammetry (CV) of modified WE **Au|butanethiol** in a 0.3 mM $Cu(OTf)_2$ solution in 100 mM pH 7 HEPES buffer under an argon atmosphere between 0.7 and 0.0 V vs RHE for 5 cycles. A subsequent 5 s dip in Milli-Q water in the dark to ensure removal of any unanchored species afforded modified WE ^{CV}**Au|butanethiol|Cu**.

^{EDTA}Au|Butanethiol. To ensure removal of all noncoordinated copper species after the introduction of copper, modified WE ^{CV}**Au|butanethiol |Cu** was immersed into a 10 mM solution of EDTA in Milli-Q water for 30 min. A subsequent 5 s dip in Milli-Q water in the dark ensured removal of any unanchored species and afforded modified WE ^{EDTA}**Au|butanethiol**.

Samples for XPS, XAS, XRD, and SEM/EDX Analyses. Electrode samples for X-ray photoelectron spectroscopy (XPS), X-ray absorption spectroscopy (XAS), X-ray diffraction (XRD), and scanning electron microscopy (SEM) combined with energy dispersive X-ray (EDX) spectroscopy were prepared from disposable Au(111) electrodes purchased from Metrohm. These electrodes were used without prior manual or electrochemical polishes. The single-crystalline character of the disposable gold electrodes oriented along the (111) plane of the face-centered cubic lattice was confirmed by XRD analysis (Figure S13). A custom-made single-compartment 5 mL PEEK cell was used for CV of the modified disposable electrodes, and samples were dried under vacuum at 70 °C for 1 h before transportation under a N_2 atmosphere. To be able to verify that the anchored Cu ions did not form a deposition directly attached to the gold surface and therefore underneath the SAM layer, another modified WE was prepared for XPS analysis. This WE contained both a Cu deposit directly attached to the gold surface and the heteromolecular SAM (**Au|Cu|mixed SAM**). The modification was prepared by chronoamperometry of a bare disposable gold electrode in a 6.6 mM $Cu(OTf)_2$ solution in 0.1 M $NaClO_4$ (99.99% purity, Merck) electrolyte under an argon atmosphere at 0.4 V for 400 s. A subsequent 5 s dip in Milli-Q water ensured removal of any unanchored species. The dip in Milli-Q water was followed by immersion of the electrode in a 2 mM solution of **5** and 1-butanethiol in a 1:1 ratio in ethanol under a N_2 atmosphere for 19 h. Final consecutive 5 s dips in ethanol and in Milli-Q water in the dark ensured removal of any unanchored hydrophobic thiol compound and of the ethanol droplet which was left behind during the ethanol wash, respectively, and afforded modified WE **Au|Cu|mixed SAM**.

X-ray Photoelectron Spectroscopy. XPS was performed on a Thermo Scientific K-Alpha spectrometer equipped with a monochromatic X-ray source and a double focusing hemispherical analyzer with a 128-channel delay line detector. Spectra were obtained by using an aluminum anode (Al Kα = 1486.6 eV) operated at 72 W with a spot size of 400 μm. Survey scans were measured at constant pass energy of 200 eV, and high-resolution scans of the separate regions were measured at 50 eV pass energy. The background pressure of the ultrahigh vacuum (UHV) chamber was 2×10^{-8} mbar, and sample charging was compensated by the use of an electron flood gun. Binding energy (BE) calibration was done by setting the C 1s peak of adventitious carbon for an unmodified disposable gold electrode at 284.8 eV. The calibrated BE of the Au 4f signal of the unmodified gold electrode was then used to calibrate all other samples. BE calibration of $Cu(OTf)_2$ and Na_2SO_4 was done by setting the C 1s peak of adventitious carbon at 284.8 eV. Modified electrode samples were transported to the UHV chamber under a N_2 atmosphere. [Cu(tmpa)(MeCN)](OTf)$_2$, ligand precursor **4**, and HEPES were measured as reference compounds by dropcasting each of them on a separate bare disposable gold WE using either water or ethanol as the solvent. CasaXPS software was used to fit the obtained spectra.

X-ray Absorption Spectroscopy. Cu K-edge XAS measurements were performed at ambient temperature at the Dutch-Belgian beamline (DUBBLE) at the European Synchrotron Radiation Facility (ESRF) in Grenoble, France. Cu foil was used as a reference for energy calibration, and all spectra were collected in fluorescence mode with a grazing incidence angle of 0.3°. [Cu(tmpa)(MeCN)](OTf)$_2$ was measured as a reference compound by dropcasting it on a bare disposable gold WE using water as the solvent. Athena software was used to process the obtained spectra with a normalization order of 2 and the Boxcar average smoothening with a kernel size of 7.[34]

X-ray Diffraction. XRD patterns were recorded under vacuum on a D8-Advance diffractometer from Bruker operating in Bragg−Brentano geometry. It was equipped with a Co Kα anode (λ = 1.78897 Å) operating at 40 kV and 30 mA, and a Lynxeye position sensitive detector. Diffraction data were collected at angles ranging from 10° to 100° with a step size of 0.02° and a scan rate of 0.2° s^{-1}. To be able to fit the samples in the sample holder, the disposable electrodes were cut into smaller sizes (Figure S12). Modified electrode sample ^{EDTA}**Au|mixed SAM|Cu** was cut under an argon atmosphere inside a glovebox and transported to the diffractometer in the dark.

Scanning Electron Microscopy. SEM images were obtained with a Thermo Scientific Apreo scanning electron microscope operating under high vacuum at an accelerating voltage of 15 kV and a beam current of 0.8 nA. The electron source was a Schottky type field emission gun, and secondary electrons were used to obtain

DOI: 10.1021/acs.inorgchem.9b01921
Inorg. Chem. 2019, 58, 13007−13019

the SEM images. A Thermo Scientific UltraDry energy dispersive X-ray (EDX) detector was used to acquire the EDX spectrum and elemental mapping at the same position of the sample as the SEM image itself. The selected settings of the microscope resulted in a dead time of 29% for the EDX detector. Thermo Scientific Pathfinder X-ray microanalysis software was used for data processing. To be able to fit the samples in the sample holder, the conductive steel wires of the disposable electrodes were cut in half. Modified electrode sample ^{EDTA}**Au\|mixed SAM\|Cu** was cut under an argon atmosphere inside a glovebox and transported to the sample chamber of the microscope in the dark.

RESULTS AND DISCUSSION

Ligand Synthesis. To enable anchoring of the Cu-tmpa complex of interest to a gold surface, the tmpa ligand was functionalized with an alkyl thiol chain (Scheme 1). The functionalization was introduced at the *ortho* position for synthetic reasons, and the overall synthesis to obtain desired thiol substituted ligand **5** consisted of five steps. The initial step of the synthetic pathway was a reductive amination of 6-bromo-2-pyridinecarboxaldehyde with di(2-picolyl)amine, which was followed by a nucleophilic aromatic substitution of the bromo substituent of the resulting substituted tmpa with partly protected dihydroxide 4-((^{t}butyldimethylsilyl)oxy)-butan-1-ol. Deprotection of the resulting ^{t}butyldimethylsilyl protected hydroxyl substituent using tetra-*n*-butylammonium fluoride (TBAF) was followed by a nucleophilic substitution of the hydroxyl moiety with a chloride. The final step was the formation of an isothiouronium intermediate which was hydrolyzed to yield thiol substituted ligand **5**.

The presence of the thiol−SH was confirmed by coupling with its methylene neighbor observed by ^{1}H^{1}H correlation spectroscopy (COSY) NMR, and ^{1}H^{13}C heteronuclear multiple bond correlation (HMBC) NMR, even though high resolution mass spectrometry (HRMS) only showed masses corresponding to the disulfide analogue of compound **5**. The NMR signal corresponding to the thiol's hydrogen was retained after prolonged exposure of compound **5** to air and ethanol or chloroform, indicating that the disulfide analogue which was observed by HRMS (see Experimental Section) must have been the result of oxidation inside the mass spectrometer.

Formation of the SAMs. In order to assign any feature to a self-assembled monolayer on gold, it is important to make sure that the gold surface is fully covered by a well-defined and close-packed SAM architecture. To counter the mismatch in size between the thioalkyl spacer and the tmpa headgroup, ligand **5** was therefore co-immobilized with butanethiol to produce a mixed SAM, as is commonly described in the literature.[20] Co-immobilization of **5** and butanethiol was achieved by immersion of the gold working electrode (WE) in an ethanolic solution of **5** and 1-butanethiol in a 1:1 molar ratio for 19−20 h. This resulted in the formation of modified WE **Au\|mixed SAM** (Scheme 2a).

After the initial anchoring of the heteromolecular SAM on the gold surface of the WE, copper was introduced into the system by cyclic voltammetry (CV) in pH 7 HEPES buffer containing $Cu(OTf)_2$ as the copper precursor (see next section for details). This resulted in the formation of modified WE ^{CV}**Au\|mixed SAM\|Cu**.

To ensure removal of all noncoordinated remnants of the introduced copper ions, the modified WE ^{CV}**Au\|mixed SAM\|Cu** was immersed into a solution of the chelating agent ethylenediaminetetraacetic acid (EDTA) in Milli-Q water for half an hour. This removal resulted in modified WE ^{EDTA}**Au\|mixed SAM\|Cu**.

Scheme 2. Schematic Overview of the Steps Involved in the Electrode Modifications (Light Gray) with the Modified Electrodes Shown in Dark Gray

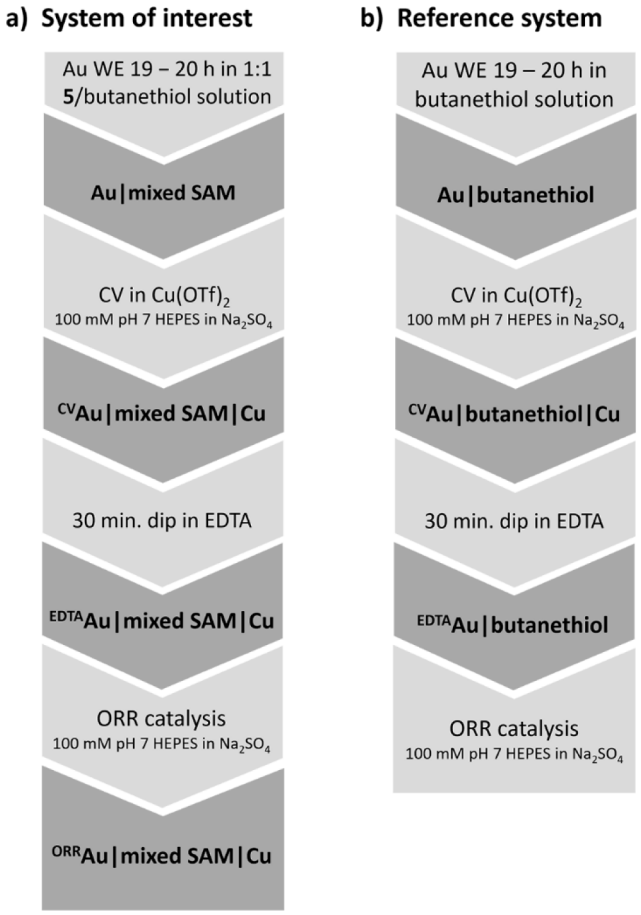

In order to pinpoint any feature of the mixed SAM system to a copper site, a second set of modified WEs was assembled. The SAM of these modified reference WEs lacked the presence of thiol functionalized tmpa ligand **5** and consisted of butanethiol only. The homomolecular SAM of the reference system was obtained by immersion of a gold WE in an ethanolic solution of only 1-butanethiol, resulting in modified WE **Au\|butanethiol** (Scheme 2b). Consecutive CV in pH 7 HEPES buffer containing $Cu(OTf)_2$ and immersion in Milli-Q water containing EDTA resulted in modified reference WEs ^{CV}**Au\|butanethiol\|Cu** and ^{EDTA}**Au\|butanethiol**, respectively.

Electrochemical Behavior. Given that a gold surface is able to catalyze the oxygen reduction reaction within a potential window where gold supported SAMs are stable, the ORR was used as a measure for the coverage of the gold surface. The lack of ORR current observed for modified WEs **Au\|mixed SAM** and **Au\|butanethiol** verified the inactivity of the gold electrode surface of the system of interest and the reference system, respectively (Figure 1 red lines vs gray lines). This inactivity demonstrates the successful complete coverage of the gold surface. After introduction of the copper ions, modified WEs ^{CV}**Au\|mixed SAM\|Cu** and ^{EDTA}**Au\|mixed SAM\|Cu** showed ORR activity with an onset at 0.5 and 0.4 V, respectively (Figure 1a blue line vs green line). A change in ORR profile and activity after the immersion of ^{CV}**Au\|mixed**

DOI: 10.1021/acs.inorgchem.9b01921
Inorg. Chem. 2019, 58, 13007−13019

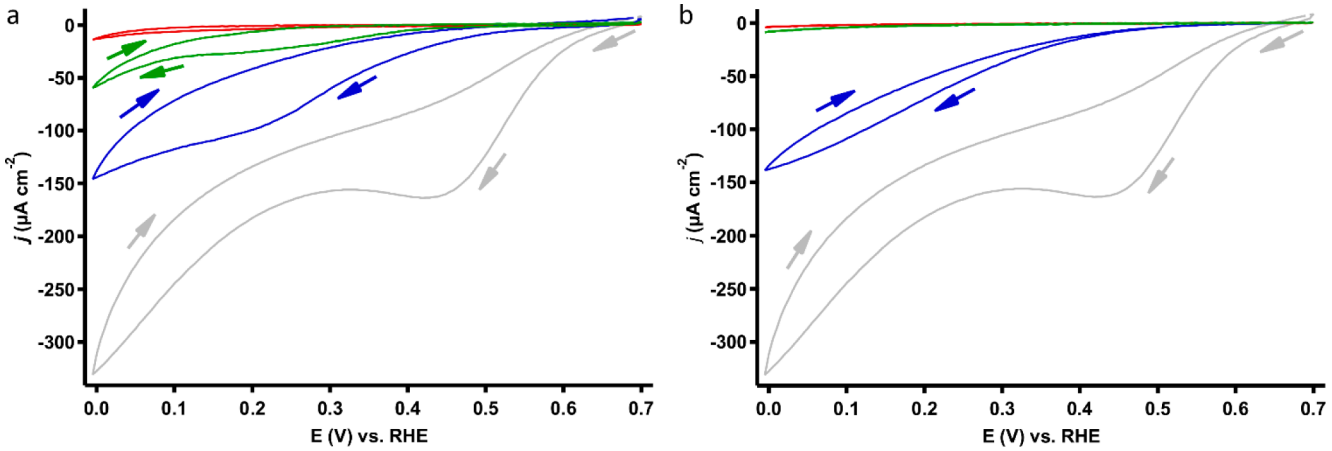

Figure 1. Cyclic voltammograms of an unmodified gold WE (gray lines) and modified WEs **Au|mixed SAM** (red line in a), ^{CV}**Au|mixed SAM|Cu** (blue line in a), ^{EDTA}**Au|mixed SAM|Cu** (green line in a), **Au|butanethiol** (red line in b), ^{CV}**Au|butanethiol|Cu** (blue line in b), and ^{EDTA}**Au|butanethiol** (green line in b) in 100 mM pH 7 HEPES buffer solution in 75 mM Na_2SO_4 electrolyte under an oxygen atmosphere at a scan rate of 100 mV s^{-1}. The modified WEs were measured in the dark. For clarity, only the third scan of all measurements is shown. The full measurements of 5 scans are shown in Figures S1 and S2.

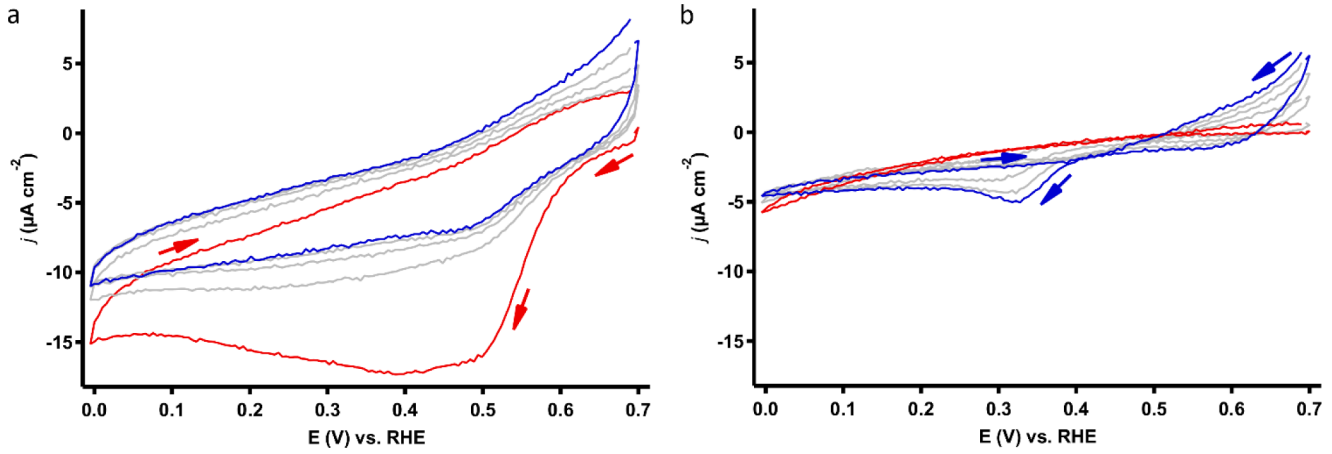

Figure 2. Cyclic voltammograms of modified WEs **Au|mixed SAM** (a) and **Au|butanethiol** (b) in 0.3 mM $Cu(OTf)_2$ in 100 mM pH 7 HEPES buffer solution in 75 mM Na_2SO_4 electrolyte under an argon atmosphere at a scan rate of 100 mV s^{-1}. The first scan is depicted as a red line. The second, third, and fourth scans are depicted as gray lines, and the fifth scan is depicted as a blue line.

SAM|Cu in an EDTA solution suggests that the EDTA changes the composition of the electrode modification by removing (some of) a catalytically active copper species from the SAM. It is important to note that both Cu-tmpa and heterogeneous copper deposits can catalyze the ORR and that the observed ORR activity of ^{EDTA}**Au|mixed SAM|Cu** is very minor compared to homogeneous Cu-tmpa.[28]

Also ^{CV}**Au|butanethiol|Cu** shows ORR activity (Figure 1b blue line). However, this activity can be completely removed by an EDTA wash; that is, ORR activity has completely disappeared in the case of ^{EDTA}**Au|butanethiol** (Figure 1b green line). This suggests that residual copper at the electrode interface that is not associated with tmpa binding is efficiently removed by the EDTA wash. The ORR activity which was observed for ^{EDTA}**Au|mixed SAM|Cu** as opposed to ^{EDTA}**Au|butanethiol** suggests that a copper species remained attached to the heteromolecular SAM and was not removed by the EDTA wash. These remaining copper sites are coordinated to the tmpa fragment via a sufficiently strong interaction and could therefore not be removed by EDTA, as expected.[35] The post ORR catalysis sample of the heteromixed SAM will be referred to as ^{ORR}**Au|mixed SAM|Cu** in further characterization studies.

After performing ORR catalysis with modified electrode sample ^{EDTA}**Au|mixed SAM|Cu**, the intactness of the coverage of the gold electrode surface was investigated. This was done by performing CV with modified electrode ^{ORR}**Au|mixed SAM|Cu** between 0.7 and −0.2 V vs RHE under an argon atmosphere. In this potential window, unmodified gold shows proton reduction activity with an onset at −0.13 V vs RHE. An absence of proton reduction current for the modified electrode validated that the surface of the gold electrode was still completely covered after ORR catalysis (Figure S3).

During the introduction of copper into modified WE **Au|mixed SAM** by CV in a $Cu(OTf)_2$ solution under an argon atmosphere, an irreversible reduction of Cu^{II} was visible at 0.45 V vs RHE in the first scan (Figure 2a). This observation suggests that electrochemical reduction of the Cu^{II} precursor present in solution initiates the formation of a reduced copper species at the electrode interface. The absence of any redox couples for the anchored Cu-tmpa-$O(CH_2)_4SH$ system when the Cu^{II} precursor is not present in solution suggests that the reduced copper species present at the electrode interface is not

DOI: 10.1021/acs.inorgchem.9b01921
Inorg. Chem. 2019, 58, 13007−13019

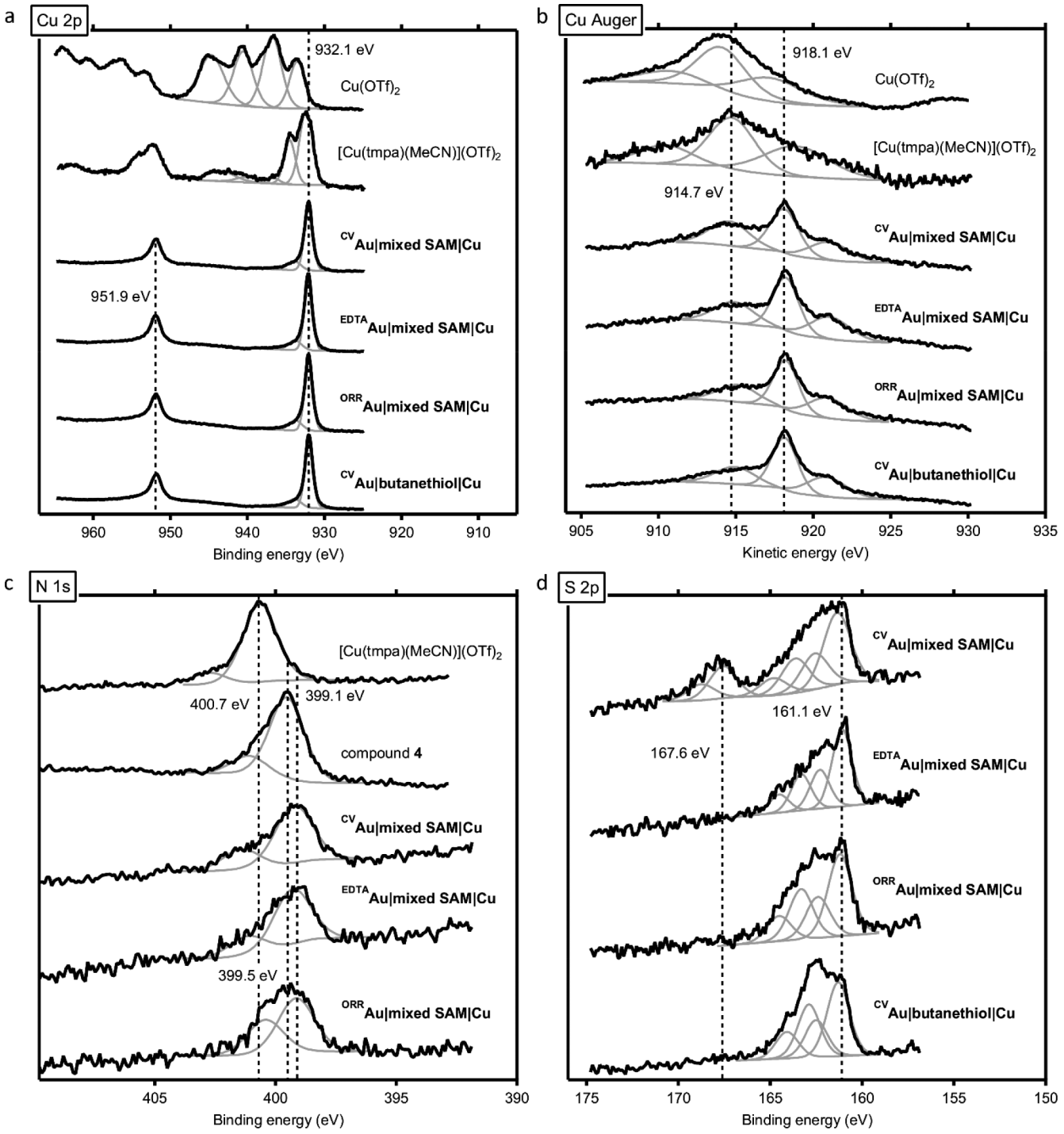

Figure 3. XPS spectra (black lines) of modified electrodes ^{CV}**Au|mixed SAM|Cu**, ^{EDTA}**Au|mixed SAM|Cu**, ^{ORR}**Au|mixed SAM|Cu**, and ^{CV}**Au|butanethiol|Cu**, and reference compounds [Cu(tmpa)(MeCN)](OTf)$_2$, Cu(OTf)$_2$, and **4**. (a) Cu 2p region, (b) Cu $L_3M_{4,5}M_{4,5}$ Auger region, (c) N 1s region, and (d) S 2p region of the XPS spectra. The deconvolution of the Cu $2p_{3/2}$, Cu $L_3M_{4,5}M_{4,5}$ Auger, N 1s, and S 2p regions is depicted in gray.

reoxidized to the +II oxidation state within a potential window between −0.2 and 0.7 V vs RHE (Figure S3 blue lines). This is in contrast to homogeneous Cu^{II}-tmpa for which a reversible redox couple with an anodic peak potential of 0.24 V vs RHE is found.[28] During CV of **Au|butanethiol** in a Cu(OTf)$_2$ solution under an argon atmosphere, no significant reduction currents were obtained apart from some minor peaks during the third scan and beyond (Figure 2b). The differences in voltammetry of **Au|butanethiol** and **Au|mixed SAM** in the presence of Cu(OTf)$_2$ together with the EDTA wash results suggest that accumulation of copper at the butanethiol SAM proceeds in a different manner than at the mixed SAM. In line with this, experiments wherein the copper was introduced by immersion of **Au|mixed SAM** in a Cu(OTf)$_2$ solution in Milli-Q water without applying a potential led to a very low copper content and poor reproducibility (vide infra). Electrochemical reduction of copper(II) with tmpa embedded in the SAM is apparently essential to obtain a stable anchored copper species.

DOI: 10.1021/acs.inorgchem.9b01921
Inorg. Chem. 2019, 58, 13007−13019

X-ray Photoelectron Spectroscopy. To determine the elemental composition of the SAMs and the oxidation state of the anchored copper species, XPS was performed on electrode samples ^{CV}**Au|mixed SAM|Cu**, ^{EDTA}**Au|mixed SAM|Cu**, ^{ORR}**Au|mixed SAM|Cu**, and ^{CV}**Au|butanethiol|Cu**. [Cu(tmpa)(MeCN)](OTf)$_2$, ligand precursor **4**, and HEPES were measured as reference compounds by dropcasting each of them on a separate bare disposable gold WE using either water or ethanol as the solvent. Cu(OTf)$_2$ and Na_2SO_4 were measured as reference compounds as well but were measured as solid powders without dropcasting.

As shown in Figure 3a, the Cu 2p$_{3/2}$ region of the XPS spectrum of the Cu(OTf)$_2$ reference compound contains two copper species with binding energies of 933.5 and 936.8 eV. These energies are in the range where Cu^{II} compounds such as CuO and Cu(OH)$_2$ are typically found.[36] The shakeup satellite features typically observed for Cu^{II} compounds are present between 939 and 950 eV. Furthermore, the Auger peak maximum at a kinetic energy (KE) of 914.0 eV in the Cu $L_3M_{4,5}M_{4,5}$ spectrum coincides with a typical Cu^{II} species as well (Figure 3b).[37] The Cu 2p$_{3/2}$ region of the XPS spectrum of reference compound [Cu(tmpa)(MeCN)](OTf)$_2$ contains two copper species as well, but these have a BE of 932.4 and 934.5 eV. Even though these BEs are slightly low for a typical Cu^{II} compound, the presence of shakeup satellite features is still visible between 938 and 948 eV. The negative shift of the Cu 2p$_{3/2}$ signals of [Cu(tmpa)(MeCN)](OTf)$_2$ compared to Cu(OTf)$_2$ suggests that the tmpa ligand has an electron donating effect on the electronic structure of the Cu^{II} ion, as one would expect. The positive shift of the Auger peak maximum from a KE of 914.0 eV for Cu(OTf)$_2$ to 914.7 eV for [Cu(tmpa)(MeCN)](OTf)$_2$ supports this hypothesis.

For all four modified electrode samples (^{CV}**Au|mixed SAM|Cu**, ^{EDTA}**Au|mixed SAM|Cu**, ^{ORR}**Au|mixed SAM|Cu**, and ^{CV}**Au|butanethiol|Cu**), only one signal with a BE of 932.1 eV is observed in the Cu 2p$_{3/2}$ region of the XPS spectrum. This energy coincides with the BE of a Cu^{I} compound such as Cu_2O.[36] According to the NIST XPS database, copper species with a BE between 932.2 and 933.2 eV can be attributed both to Cu(0) and various Cu(I) species.[37] The absence of the characteristic satellite features in the Cu 2p$_{3/2}$ region of the XPS spectra also indicates the presence of either a Cu^0 or a Cu^I species at the gold electrode surface. The high KE of 918.1 eV for the Auger peak maximum in the Cu $L_3M_{4,5}M_{4,5}$ spectra of the four modified electrode samples seems to suggest that the anchored copper is a Cu^0 species rather than a Cu^I species.[37] However, to the best of our knowledge, no XPS data have been reported for Cu^I coordination complexes, making it rather difficult to make a relevant comparison to our modified electrode samples. Whether the oxidation state of the Cu ion of the anchored complex on the gold electrode surface is +I or +0 could therefore not be determined on the basis of XPS analysis alone.

Both the BE of the signal in the Cu 2p$_{3/2}$ region of the XPS spectrum and the KE of the Auger peak maximum in the Cu $L_3M_{4,5}M_{4,5}$ spectrum of ^{CV}**Au|butanethiol|Cu** coincide with the same energies of ^{CV}**Au|mixed SAM|Cu**, ^{EDTA}**Au|mixed SAM|Cu**, and ^{ORR}**Au|mixed SAM|Cu**. This overlap shows that the copper ion of the anchored complex of interest and the residual copper species are similar on the basis of XPS. Since the latter could be removed by EDTA (*vide supra*), whereas the former could not, it can be concluded that they are in fact not the same at all.

It is important to verify that the copper is located on top of the SAM in close proximity to the tmpa N-donors and not underneath the SAM at the gold interface. To rule out such a latter arrangement, an additional sample (**Au|Cu|mixed SAM**) was prepared and analyzed by XPS. This sample contained both a Cu deposit directly on the gold surface, and the heteromolecular SAM. The Cu deposit was formed by chronoamperometry in a Cu(OTf)$_2$ solution under an argon atmosphere at 0.4 V for 400 s. Subsequent immersion of the electrode in an ethanolic solution of **5** and 1-butanethiol in a 1:1 molar ratio for 19 h introduced the heteromolecular SAM and resulted in modified electrode **Au|Cu|mixed SAM**. As shown in Figure S4a, the BE of the signal in the Cu 2p$_{3/2}$ region of the XPS spectrum of **Au|Cu|mixed SAM** is shifted by only 0.3 eV compared to ^{CV}**Au|mixed SAM|Cu**, ^{EDTA}**Au|mixed SAM|Cu**, ^{ORR}**Au|mixed SAM|Cu**, and ^{CV}**Au|butanethiol|Cu**. A more pronounced shift of 1.2 eV was observed for the KE of the Auger peak maximum in the Cu $L_3M_{4,5}M_{4,5}$ spectrum of **Au|Cu|mixed SAM** (Figure S4b). This clear difference in KE of the Auger peak maximum indicates that the observed copper species for ^{CV}**Au|mixed SAM|Cu**, ^{EDTA}**Au|mixed SAM|Cu**, ^{ORR}**Au|mixed SAM|Cu**, and ^{CV}**Au|butanethiol|Cu** is not a deposition which is formed directly onto the surface of the gold electrode. A quantitative analysis of the XPS data further confirms the lack of resemblance between the **Au|Cu|mixed SAM** sample and modified electrodes ^{CV}**Au|mixed SAM|Cu**, ^{EDTA}**Au|mixed SAM|Cu**, and ^{ORR}**Au|mixed SAM|Cu** (Table S1).

The N 1s regions of the XPS spectra of reference compounds [Cu(tmpa)(MeCN)](OTf)$_2$ and ligand precursor **4** show signals with a BE of 400.7 and 399.5 eV, respectively (Figure 3c). The negative shift of 1.2 eV indicates that the introduction of the substituent on the tmpa ligand has a relatively large effect on the observed BE of the nitrogen originating from the ligand. This effect is most likely caused by the electron donating properties of the ether functionality. For modified electrode samples ^{CV}**Au|mixed SAM|Cu**, ^{EDTA}**Au|mixed SAM|Cu**, and ^{ORR}**Au|mixed SAM|Cu**, the BE of the same signal in the N 1s region of the XPS spectrum is shifted slightly more negative to 399.1 eV. This further negative shift compared to unanchored compound **4** might be explained by the electron donating properties of the bulk gold metal to which thiol substituted tmpa ligand **5** was anchored.

The S 2p region of the XPS spectrum of modified electrode sample ^{CV}**Au|mixed SAM|Cu** shows the presence of an additional sulfur containing species compared to the ^{EDTA}**Au|mixed SAM|Cu**, ^{ORR}**Au|mixed SAM|Cu**, and ^{CV}**Au|butanethiol|Cu** modified electrode samples (Figure 3d). The BE of the signal of this additional sulfur containing species amounts to 167.6 eV and does not coincide with either HEPES or Na_2SO_4 (Figure S5). Lack of the additional signal in the ^{EDTA}**Au|mixed SAM|Cu** sample shows, however, that the corresponding species is completely removed by the EDTA wash. Furthermore, no sulfate signals were observed in the S 2p region of the XPS spectra of the modified electrodes.[35]

Quantitative XPS analysis was employed to determine the elemental ratios for the anchored system of interest after the removal of the excess copper species. In the case of both modified electrode samples ^{EDTA}**Au|mixed SAM|Cu** and ^{ORR}**Au|mixed SAM|Cu**, this analysis resulted in elemental ratios of ~3:2 and ~7:2 for nitrogen to copper and sulfur to copper, respectively (Table 1). These ratios indicate that every

DOI: 10.1021/acs.inorgchem.9b01921
Inorg. Chem. 2019, 58, 13007−13019

Table 1. Ratio of Nitrogen to Copper Species and Sulfur to Copper Species of the Modified Electrodes and the Reference Compound $[Cu(tmpa)(MeCN)](OTf)_2$ as Determined by XPS

Sample	Elemental ratio N:Cu[a]	Elemental ratio S:Cu[a]
^{CV}**Au|mixed SAM|Cu**	1.9	3.8
^{EDTA}**Au|mixed SAM|Cu**	1.4[b]	3.4[b]
^{ORR}**Au|mixed SAM|Cu**	1.5[b]	3.9[b]
$[Cu(tmpa)(MeCN)](OTf)_2$	4.7[c]	N/A

[a]The total area of all species in the N 1s region was used to determine the ratios. For the modified electrodes, the total area of all species in the S 2p region with a BE between 159 and 166 eV and the area of the Cu $2p_{3/2}$ signal at BE = 932.1 eV were used to determine the ratios. For $[Cu(tmpa)(MeCN)](OTf)_2$, the total area of the Cu $2p_{3/2}$ signals at BE = 932.4, 934.5, and 936.7 eV was used to determine the ratios. [b]Average of two measurements (see Table S2). [c]Elemental analysis revealed an actual composition of $[Cu(tmpa)](OTf)_2$ + 0.7 MeCN + 0.9 H_2O for $[Cu(tmpa)(MeCN)](OTf)_2$.[28]

tmpa ligand binds to roughly two to three copper ions once it is anchored to the gold surface and more or less every ninth thiolate moiety consists of functionalized tmpa ligand **5**.

X-ray Absorption Spectroscopy. To be able to differentiate between molecular Cu^I and Cu^0 species for our anchored system of interest, grazing incidence X-ray absorption spectroscopy (XAS) was performed on modified electrode sample ^{EDTA}**Au\|mixed SAM\|Cu**. This study particularly focused on the Cu K-edge X-ray absorption near-edge structure (XANES) region of the X-ray absorption spectrum as this technique provided sufficient sensitivity to assign the oxidation state of the ^{EDTA}**Au\|mixed SAM\|Cu** sample, despite the presence of only a monolayer of material. Elucidation of the oxidation state by XANES has previously been performed for enzymatic and molecular copper sites and showed quite pronounced shifts in onset energy of the edge position for changes in the oxidation state of the metal ion. Consequently, a plethora of reference samples of well-defined molecular copper(I)[38−45] and copper(II)[38,45−47] sites is available.

Since modified electrode sample ^{EDTA}**Au\|mixed SAM\|Cu** contains only a monolayer of anchored material, a low intensity XANES spectrum was obtained. Boxcar average smoothing of the XANES spectrum of ^{EDTA}**Au\|mixed SAM\|Cu** (Figure S6) allowed for qualitative analysis and a valid comparison with various relevant references. The negative shift of the absorption edge of the modified electrode compared to the absorption edge of a $[Cu(tmpa)(MeCN)](OTf)_2$ reference sample confirms that the species present at the modified electrode is not a Cu^{II} species (Figure 4 bold blue line vs red line). In addition to the $[Cu(tmpa)(MeCN)](OTf)_2$ reference sample, literature based reference spectra of a distorted trigonal bipyramidal Cu^{II} complex and 13 Cu^I complexes are shown (complex 1 and complexes 2−14 in Figure S8).[38−42] The XANES spectrum of the molecular Cu^{II} reference complex has been reported in the literature as a typical Cu^{II} spectrum, selected from a list of 40 Cu^{II} coordination complexes.[38] The 13 Cu^I reference complexes have previously been selected from the literature by Hodgson et al. due to their variety in geometry, coordination number, and ligand structure, resulting in shifts in the onset energy of the edge position (Figure S7 and S8).[38−42] The alignment of the absorption edges of the Cu^I reference complexes and the absorption edge of the modified electrode shows that the anchored Cu-tmpa-

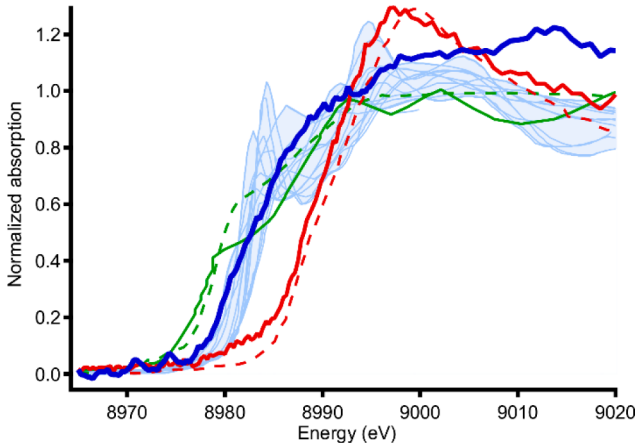

Figure 4. XANES region of the Cu K-edge XAS spectra measured for ^{EDTA}**Au\|mixed SAM\|Cu** (bold blue line) and $[Cu(tmpa)(MeCN)](OTf)_2$ (red line). Reference spectra from the literature of a distorted trigonal bipyramidal Cu^{II} complex[38] (red dashed line, complex 1 in Figure S8), 13 Cu^I complexes[38−42] (thin blue lines, complexes 2−14 in Figure S8), metallic copper[48] (green line), and Cu^0 nanoparticles[49] (dashed green line) are depicted as well. The spectral data of the red dashed line was reprinted and adapted with permission from ref 36. Copyright 1987 American Chemical Society. The spectral data of the thin blue lines was reprinted and adapted with permission from refs 36−40. Copyright 1987 American Chemical Society, 1996 John Wiley and Sons, 2013 American Chemical Society, 2013 Taylor & Francis, 2014 American Chemical Society, respectively. The spectral data of the green line was reprinted and adapted with permission from ref 46. Copyright 2013 Elsevier. The spectral data of the dashed green line was reprinted and adapted with permission from ref 47. Copyright 2018 John Wiley and Sons. The data was extracted using ScanIt.[50] The shown spectrum of ^{EDTA}**Au\|mixed SAM\|Cu** is a smoothed fit of the raw data (Figure S6).

$O(CH_2)_4SH$ system is a Cu^I species rather than a Cu^{II} species. Usually, distinct Cu^I species show the presence of a well-defined rising edge feature.[38] For the 13 Cu^I reference complexes, this rising edge feature is visible between 8982.9 and 8986.7 eV. The absence of the rising edge feature in the XANES spectrum measured for ^{EDTA}**Au\|mixed SAM\|Cu** might be the result of broadness of the XANES data caused by heterogeneity of the sample. Further comparison of the XANES spectrum of ^{EDTA}**Au\|mixed SAM\|Cu** with XANES data obtained from the literature for metallic copper and Cu^0 nanoparticles shows a significant negative shift of the onset energy of the absorption edge for both Cu^0 references (Figure 4 green line and dashed green line).[48,49] This shift supports an assignment of the +I oxidation state for the anchored copper species and rules out the +0 oxidation state. The relatively low onset energy of the absorption edge observed for modified electrode ^{EDTA}**Au\|mixed SAM\|Cu** might, however, be the result of the presence of a minor Cu^0 species besides the major Cu^I species. A final comparison with the XANES data of a reference spectrum of Cu_2O shows a significant negative shift of the onset energy of the absorption edge as well, confirming that the anchored Cu^I species of interest is a molecular architecture rather than cuprous oxide (Figure S9 dotted green line).[48]

Scanning Electron Microscopy. To verify whether accumulated copper particles were present on the surface of the modified gold electrode, ^{EDTA}**Au\|mixed SAM\|Cu** was analyzed by a combination of scanning electron microscopy (SEM) imaging and energy dispersive X-ray (EDX) spectros-

DOI: 10.1021/acs.inorgchem.9b01921
Inorg. Chem. 2019, 58, 13007−13019

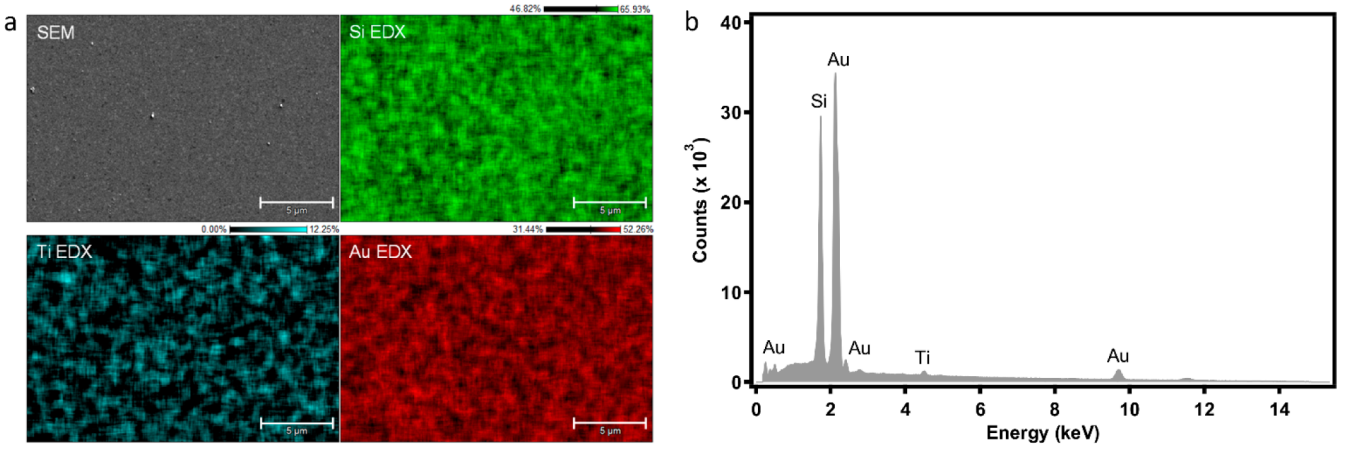

Figure 5. SEM image, quantitative elemental mapping (a), and EDX spectrum (b) of modified electrode ^{EDTA}**Au|mixed SAM|Cu**. Scale bars in a are 5 μm.

copy. The SEM images of both the modified electrode and an unmodified gold electrode (Figure S10 and S11a, c, and e) are qualitatively the same. The surfaces are very uniform apart from small particles that are present at both electrode surfaces. While the detection limit of the EDX spectrometer is not sufficient to detect the presence of a submonolayer of metal ions, accumulated metal particles should be detectable. The EDX spectrum and elemental mapping which were acquired at the same position of the sample as the SEM image did, however, not show the presence of any copper (Figure 5a and b), neither at the uniform surface nor at the scattered particles (Figure S10c,e). This confirms that no accumulation of copper material was present on the surface of the modified electrode. The observed silicon, titanium, and gold can be assigned to the quartz, TiO_2 layer, and gold layer of the disposable electrode, respectively.

X-ray diffraction (XRD) analysis of a fresh prepared ^{EDTA}**Au|mixed SAM|Cu** sample confirmed that the modification on the gold surface does not contain an accumulation of crystalline copper material (Figure S13).

Structure of Modification. The quantitative XPS results of elemental ratios of ~3:2 nitrogen to copper species and ~7:2 sulfur to copper species indicate that more than two Cu ions are present for each anchored tmpa ligand. These ratios suggest that each ligand is coordinated to two copper ions and that additional bridging copper ions might be present in the modification of the gold surface as well. The formation of the bridging copper ions is most likely facilitated by two circumstances: (a) a relatively high tmpa ligand density at the gold surface which leads to close proximity of the neighboring tmpa ligands, and (b) a high excess of copper present in solution during the introduction of copper compared to the amount of ligand present at the gold surface. Deviations from the elemental ratios in the observed experimental values can be explained by a modification which is not completely uniformly distributed along the gold surface (Table S2). Additionally, formation of more or less bridging copper ions between some ligands might explain a deviation in elemental ratio along the gold surface. Taking the elemental ratios into account, we suggest a schematic representation of the modification on the gold surface as depicted in Figure 6. An extensive list of published crystal structures of tetranuclear copper units shows that both Cu^{II} and Cu^{I} complexes containing a Cu_4O_4 core often assemble into a tetramer cubic structure.[51−58] Therefore, it seems likely that the bridging copper ions are arranged in a cubane type of structure with water as the coordinating solvent and hydroxide as the coordinating counterion (L = H_2O and X = OH^- in Figure 6). The presence of these bridging copper ions would result in the formation of a polymeric coordination complex.

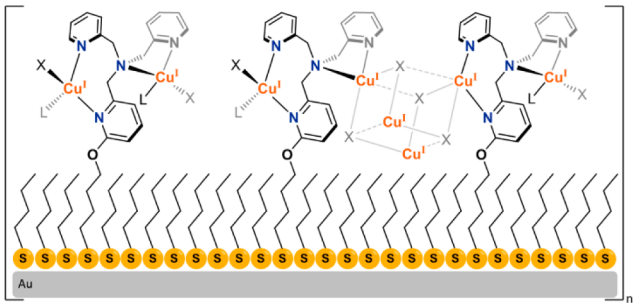

Figure 6. Schematic representation of the modification on the gold surface taking into account the elemental ratios and oxidation state assignment on the basis of XPS and XANES. In analogy with the structural arrangements of the Cu_4O_4 core of tetranuclear copper units into a tetramer cubic structure,[51−58] a cubane type of arrangement of the bridging copper ions with water as the coordinating solvent and hydroxide as the coordinating counterion (L = H_2O and X = OH^-) seems likely.

The XANES region of the X-ray absorption spectrum confirmed the +I oxidation state of the copper ions which are present in the anchored system of interest. The stability of the anchored Cu^{I} species was already confirmed during initial electrochemical investigation; the Cu^{II} precursor was irreversibly reduced during introduction of copper into the system of interest, and the anchored system did not show any redox couples which are typically observed for homogeneous coordination complexes. To understand whether the electrochemical reduction of the Cu^{II} precursor was required for formation of the stable Cu^{I} species upon anchoring, the introduction of the Cu ions to the modified electrode was also performed by immersion in a $Cu(OTf)_2$ solution without applying a potential. The result of the Auger analysis of this sample reveals that the initial electrochemical reduction of the Cu^{II} precursor is indeed required for formation of the anchored stable Cu^{I} complex (Figure S14b). The absence of reoxidation of the anchored coordination polymer to the air stable Cu^{II} state is probably the result of the geometrical changes of the

DOI: 10.1021/acs.inorgchem.9b01921
Inorg. Chem. 2019, 58, 13007−13019

system due to coordination of each tmpa ligand to two Cu ions. The observation of ORR activity of the anchored coordination polymer, although very minimal, might be caused by a very small amount of anchored intact Cu-tmpa along the unevenly distributed modification on the gold surface.

Formation of a stable Cu^{I} species attached to a gold surface *via* a SAM has recently been observed by Ballav et al. as well, albeit under different conditions.[59] The Cu^{I} species was attached to a carboxylic acid functionalized gold thiolate alkyl chain cross-linked via bridging ferrocyanides. In the Cu $2p_{3/2}$ region of the XPS spectrum of the stabilized Cu^{I} species, only one signal with a BE of 932.0 eV was observed without the presence of any satellite features. This BE is very comparable to the BE of 932.1 eV which we observed in the Cu $2p_{3/2}$ region of the XPS spectrum of our anchored Cu^{I} species of interest. In addition to the XAS results, this comparable BE provides another confirmation for the +I oxidation state of our immobilized copper species.

CONCLUSION

XPS and XAS analyses of a Cu-tmpa-$O(CH_2)_4SH$ complex anchored to gold *via* a heteromolecular SAM have indicated that both the oxidation state and the structure of the anchored complex do not correspond to the homogeneous Cu^{II}-tmpa complex in solution. For the anchored species, a stabilized molecular Cu^{I} system was observed with an elemental ratio of ~3:2 for nitrogen to copper. The observed +I oxidation state is quite remarkable, since Cu^{I} complexes are usually very unstable and readily oxidized to air stable Cu^{II} analogues. Especially when ligated to tmpa, Cu^{I} reacts very fast with dioxygen[60] and is capable to catalyze the ORR with more than a million turnovers per second.[28] The difference in structure and oxidation state of the homogeneous and heterogenized systems shows that it cannot just be assumed that the same coordination geometries are obtained in solution and upon anchoring to a metal surface. The results of this study indicate that a correct elucidation of the actual structure of transition metal complexes upon anchoring to a surface is of utmost importance and should be a standard in the field of heterogenized coordination chemistry.

ASSOCIATED CONTENT

Supporting Information

The Supporting Information is available free of charge on the ACS Publications website at DOI: 10.1021/acs.inorgchem.9b01921.

Full cyclic voltammograms recorded under an oxygen atmosphere, proton reduction test after ORR catalysis, XPS analysis of electrode sample **Au|Cu|mixed SAM**, XPS analysis of the S 2p region of HEPES and Na_2SO_4, quantitative XPS results, raw XANES spectrum of modified electrode ^{EDTA}**Au|mixed SAM|Cu**, XANES spectra, and structures of reference Cu^{I} complexes, XANES spectra of more copper references, SEM images and EDX spectra, XRD analysis, XPS analysis of electrode sample $^{NoCV|EDTA}$**Au|mixed SAM|Cu**, and NMR spectra of compounds **1**−**5** (PDF)

AUTHOR INFORMATION

Corresponding Author

*E-mail: d.g.h.hetterscheid@chem.leidenuniv.nl.

ORCID

Jan P. Hofmann: 0000-0002-5765-1096

Dennis G. H. Hetterscheid: 0000-0001-5640-4416

Present Address

[§](L.W.) [1]Aix Marseille Université, CNRS, IM2NP UMR 7334, 13397 Marseille, France. [2]ID01/ESRF, 6 rue Jules Horowitz, BP220, F-38043 Grenoble Cedex, France.

Notes

The authors declare no competing financial interest.

ACKNOWLEDGMENTS

Financial support was provided by the European Research Council (ERC starting grant 637556 Cu4Energy to D.G.H. Hetterscheid). N.W.G. Smits gratefully acknowledges Michiel Langerman for providing the $[Cu(tmpa)(MeCN)](OTf)_2$ complex which was used for XPS and XAS measurements, Hans van den Elst for performing the HRMS analyses, Dr. Wen Tian Fu for performing the XRD measurements, Pauline van Deursen for performing the SEM/EDX measurements, and Thomas Mechielsen for help with the SEM/EDX measurements. L. Wu and J.P. Hofmann acknowledge funding from The Netherlands Organization for Scientific Research (NWO) and cofinancing by Shell Global Solutions International B.V. for the project 13CO2-6. The authors gratefully acknowledge Dr. Alessandro Longo (BM26 (DUBBLE), European Synchrotron Radiation Facility (ESRF)) and Dr. Lu Gao (Eindhoven University of Technology, TU/e) for their support during XAS measurements.

REFERENCES

(1) Amao, Y. Probes and polymers for optical sensing of oxygen. *Microchim. Acta* **2003**, *143*, 1−12.

(2) Salimi, A.; Kavosi, B.; Babaei, A.; Hallaj, R. Electrosorption of os(iii)-complex at single-wall carbon nanotubes immobilized on a glassy carbon electrode: Application to nanomolar detection of bromate, periodate and iodate. *Anal. Chim. Acta* **2008**, *618*, 43−53.

(3) Machini, W. B. S.; Teixeira, M. F. S. Electrochemical properties of the oxo-manganese-phenanthroline complex immobilized on ion-exchange polymeric film and its application as biomimetic sensor for sulfite ions. *Electroanalysis* **2014**, *26*, 2182−2190.

(4) Mayuri, P.; Saravanan, N.; Senthil Kumar, A. A bioinspired copper 2,2-bipyridyl complex immobilized mwcnt modified electrode prepared by a new strategy for elegant electrocatalytic reduction and sensing of hydrogen peroxide. *Electrochim. Acta* **2017**, *240*, 522−533.

(5) Clifford, J. N.; Martínez-Ferrero, E.; Viterisi, A.; Palomares, E. Sensitizer molecular structure-device efficiency relationship in dye sensitized solar cells. *Chem. Soc. Rev.* **2011**, *40*, 1635−1646.

(6) Song, W.; Glasson, C. R. K.; Luo, H.; Hanson, K.; Brennaman, M. K.; Concepcion, J. J.; Meyer, T. J. Photoinduced stepwise oxidative activation of a chromophore−catalyst assembly on tio2. *J. Phys. Chem. Lett.* **2011**, *2*, 1808−1813.

(7) Brown, A. M.; Antila, L. J.; Mirmohades, M.; Pullen, S.; Ott, S.; Hammarström, L. Ultrafast electron transfer between dye and catalyst on a mesoporous nio surface. *J. Am. Chem. Soc.* **2016**, *138*, 8060−8063.

(8) Ngweniform, P.; Abbineni, G.; Cao, B.; Mao, C. Self-assembly of drug-loaded liposomes on genetically engineered target-recognizing m13 phage: A novel nanocarrier for targeted drug delivery. *Small* **2009**, *5*, 1963−1969.

(9) Ruggiero, E.; Garino, C.; Mareque-Rivas, J. C.; Habtemariam, A.; Salassa, L. Upconverting nanoparticles prompt remote near-infrared photoactivation of ru(ii)−arene complexes. *Chem. - Eur. J.* **2016**, *22*, 2801−2811.

(10) Dubois, K. D.; Petushkov, A.; Garcia Cardona, E.; Larsen, S. C.; Li, G. Adsorption and photochemical properties of a molecular co2

DOI: 10.1021/acs.inorgchem.9b01921
Inorg. Chem. 2019, 58, 13007−13019

reduction catalyst in hierarchical mesoporous zsm-5: An in situ ftir study. *J. Phys. Chem. Lett.* **2012**, *3*, 486−492.
(11) Chatterjee, S.; Sengupta, K.; Hematian, S.; Karlin, K. D.; Dey, A. Electrocatalytic o2-reduction by synthetic cytochrome c oxidase mimics: Identification of a "bridging peroxo" intermediate involved in facile 4e−/4h+ o2-reduction. *J. Am. Chem. Soc.* **2015**, *137*, 12897−12905.
(12) Yagi, M.; Kinoshita, K.; Kaneko, M. Activity analysis of electrochemical water oxidation catalyst confined in a coated-polymer membrane. *J. Phys. Chem.* **1996**, *100*, 11098−11100.
(13) Karimi, B.; Enders, D. New n-heterocyclic carbene palladium complex/ionic liquid matrix immobilized on silica: Application as recoverable catalyst for the heck reaction. *Org. Lett.* **2006**, *8*, 1237−1240.
(14) Collman, J. P.; Devaraj, N. K.; Decréau, R. A.; Yang, Y.; Yan, Y.-L.; Ebina, W.; Eberspacher, T. A.; Chidsey, C. E. D. A cytochrome c oxidase model catalyzes oxygen to water reduction under rate-limiting electron flux. *Science* **2007**, *315*, 1565−1568.
(15) Kang, P.; Zhang, S.; Meyer, T. J.; Brookhart, M. Rapid selective electrocatalytic reduction of carbon dioxide to formate by an iridium pincer catalyst immobilized on carbon nanotube electrodes. *Angew. Chem., Int. Ed.* **2014**, *53*, 8709−8713.
(16) Hübner, S.; de Vries, J. G.; Farina, V. Why does industry not use immobilized transition metal complexes as catalysts? *Adv. Synth. Catal.* **2016**, *358*, 3−25.
(17) Liu, X.; Inagaki, S.; Gong, J. Heterogeneous molecular systems for photocatalytic co2 reduction with water oxidation. *Angew. Chem., Int. Ed.* **2016**, *55*, 14924−14950.
(18) Huang, J.; Liu, S.; Ma, Y.; Cai, J. Chiral salen mn (iii) immobilized on znps-pvpa through alkoxyl-triazole for superior performance catalyst in asymmetric epoxidation of unfunctionalized olefins. *J. Organomet. Chem.* **2019**, *886*, 27−33.
(19) Khajehzadeh, M.; Moghadam, M.; Jamehbozorgi, S. Synthesis and characterization of a new poly(n−heterocyclic carbene cu complex) immobilized on nano−silica, (cuii−nhcs)n@nsio2, and its application as an efficient and reusable catalyst in the synthesis of benzimidazoles, benzothiazoles, 1,2,3−triazoles, bis−triazoles and sonogashira−hagihara reactions. *Inorg. Chim. Acta* **2019**, *485*, 173−189.
(20) Love, J. C.; Estroff, L. A.; Kriebel, J. K.; Nuzzo, R. G.; Whitesides, G. M. Self-assembled monolayers of thiolates on metals as a form of nanotechnology. *Chem. Rev. (Washington, DC, U. S.)* **2005**, *105*, 1103−1170.
(21) Jia, H.-L.; Peng, Z.-J.; Li, S.-S.; Huang, C.-Y.; Guan, M.-Y. Self-assembly by coordination with organic antenna chromophores for dye-sensitized solar cells. *ACS Appl. Mater. Interfaces* **2019**, *11*, 15845−15852.
(22) Zou, S.; Clegg, R. S.; Anson, F. C. Attachment of cobalt "picket fence" porphyrin to the surface of gold electrodes coated with 1-(10-mercaptodecyl)imidazole. *Langmuir* **2002**, *18*, 3241−3246.
(23) Eckenhoff, W. T.; Pintauer, T. Atom transfer radical addition in the presence of catalytic amounts of copper(i/ii) complexes with tris(2-pyridylmethyl)amine. *Inorg. Chem.* **2007**, *46*, 5844−5846.
(24) Karlin, K. D.; Kaderli, S.; Zuberbühler, A. D. Kinetics and thermodynamics of copper(i)/dioxygen interaction. *Acc. Chem. Res.* **1997**, *30*, 139−147.
(25) Fukuzumi, S.; Kotani, H.; Lucas, H. R.; Doi, K.; Suenobu, T.; Peterson, R. L.; Karlin, K. D. Mononuclear copper complex-catalyzed four-electron reduction of oxygen. *J. Am. Chem. Soc.* **2010**, *132*, 6874−6875.
(26) Asahi, M.; Yamazaki, S.-i.; Itoh, S.; Ioroi, T. Electrochemical reduction of dioxygen by copper complexes with pyridylalkylamine ligands dissolved in aqueous buffer solution: The relationship between activity and redox potential. *Dalton Trans.* **2014**, *43*, 10705−10709.
(27) Asahi, M.; Yamazaki, S.-i.; Itoh, S.; Ioroi, T. Acid-base and redox equilibria of a tris(2-pyridylmethyl)amine copper complex; their effects on electrocatalytic oxygen reduction by the complex. *Electrochim. Acta* **2016**, *211*, 193−198.
(28) Langerman, M.; Hetterscheid, D. G. H. Very fast oxygen reduction catalysis by cu-tmpa via a stepwise mechanism. *Angew. Chem., Int. Ed.* **2019**, *58*, 12974−12978.
(29) Thorseth, M. A.; Letko, C. S.; Rauchfuss, T. B.; Gewirth, A. A. Dioxygen and hydrogen peroxide reduction with hemocyanin model complexes. *Inorg. Chem.* **2011**, *50*, 6158−6162.
(30) Ward, A. L.; Elbaz, L.; Kerr, J. B.; Arnold, J. Nonprecious metal catalysts for fuel cell applications: Electrochemical dioxygen activation by a series of first row transition metal tris(2-pyridylmethyl)amine complexes. *Inorg. Chem.* **2012**, *51*, 4694−4706.
(31) Thorseth, M. A.; Letko, C. S.; Tse, E. C. M.; Rauchfuss, T. B.; Gewirth, A. A. Ligand effects on the overpotential for dioxygen reduction by tris(2-pyridylmethyl)amine derivatives. *Inorg. Chem.* **2013**, *52*, 628−634.
(32) Trasatti, S.; Petrii, O. A. Real surface area measurements in electrochemistry. *J. Electroanal. Chem.* **1992**, *327*, 353−376.
(33) Hutt, D. A.; Leggett, G. J. Influence of adsorbate ordering on rates of uv photooxidation of self-assembled monolayers. *J. Phys. Chem.* **1996**, *100*, 6657−6662.
(34) Ravel, B.; Newville, M. Athena, artemis, hephaestus: Data analysis for x-ray absorption spectroscopy using ifeffit. *J. Synchrotron Radiat.* **2005**, *2005*, 537−541.
(35) Humphreys, K. J.; Johnson, A. E.; Karlin, K. D.; Rokita, S. E. Oxidative strand scission of nucleic acids by a multinuclear copper(ii) complex. *JBIC, J. Biol. Inorg. Chem.* **2002**, *7*, 835−842.
(36) Biesinger, M. C.; Lau, L. W. M.; Gerson, A. R.; Smart, R. S. C. Resolving surface chemical states in xps analysis of first row transition metals, oxides and hydroxides: Sc, ti, v, cu and zn. *Appl. Surf. Sci.* **2010**, *257*, 887−898.
(37) NIST X-ray Photoelectron Spectroscopy Database, version 4.1 (National Institute of Standards and Technology, Gaithersburg, USA, 2012); https://srdata.nist.gov/xps/.
(38) Kau, L. S.; Spira-Solomon, D. J.; Penner-Hahn, J. E.; Hodgson, K. O.; Solomon, E. I. X-ray absorption edge determination of the oxidation state and coordination number of copper. Application to the type 3 site in rhus vernicifera laccase and its reaction with oxygen. *J. Am. Chem. Soc.* **1987**, *109*, 6433−6442.
(39) Corazza, A.; Harvey, I.; Sadler, P. J. 1h, 13c-nmr and x-ray absorption studies of copper(i) glutathione complexes. *Eur. J. Biochem.* **1996**, *236*, 697−705.
(40) Penfold, T. J.; Karlsson, S.; Capano, G.; Lima, F. A.; Rittmann, J.; Reinhard, M.; Rittmann-Frank, M. H.; Braem, O.; Baranoff, E.; Abela, R.; Tavernelli, I.; Rothlisberger, U.; Milne, C. J.; Chergui, M. Solvent-induced luminescence quenching: Static and time-resolved x-ray absorption spectroscopy of a copper(i) phenanthroline complex. *J. Phys. Chem. A* **2013**, *117*, 4591−4601.
(41) Gaur, A.; Shrivastava, B. D. Speciation of mixtures of copper (i) and copper (ii) mixed ligand complexes by x-ray absorption fine structure spectroscopy. *Spectrosc. Lett.* **2013**, *46*, 375−383.
(42) Zhang, G.; Yi, H.; Zhang, G.; Deng, Y.; Bai, R.; Zhang, H.; Miller, J. T.; Kropf, A. J.; Bunel, E. E.; Lei, A. Direct observation of reduction of cu(ii) to cu(i) by terminal alkynes. *J. Am. Chem. Soc.* **2014**, *136*, 924−926.
(43) Harkins, S. B.; Mankad, N. P.; Miller, A. J. M.; Szilagyi, R. K.; Peters, J. C. Probing the electronic structures of [cu2(μ-xr2)]n+ diamond cores as a function of the bridging x atom (x = n or p) and charge (n = 0, 1, 2). *J. Am. Chem. Soc.* **2008**, *130*, 3478−3485.
(44) Mankad, N. P.; Antholine, W. E.; Szilagyi, R. K.; Peters, J. C. Three-coordinate copper(i) amido and aminyl radical complexes. *J. Am. Chem. Soc.* **2009**, *131*, 3878−3880.
(45) Tomson, N. C.; Williams, K. D.; Dai, X.; Sproules, S.; DeBeer, S.; Warren, T. H.; Wieghardt, K. Re-evaluating the cu k pre-edge xas transition in complexes with covalent metal−ligand interactions. *Chem. Sci.* **2015**, *6*, 2474−2487.
(46) Kundu, S.; Miceli, E.; Farquhar, E.; Pfaff, F. F.; Kuhlmann, U.; Hildebrandt, P.; Braun, B.; Greco, C.; Ray, K. Lewis acid trapping of an elusive copper−tosylnitrene intermediate using scandium triflate. *J. Am. Chem. Soc.* **2012**, *134*, 14710−14713.

DOI: 10.1021/acs.inorgchem.9b01921
Inorg. Chem. 2019, 58, 13007−13019

(47) Blusch, L. K.; Craigo, K. E.; Martin-Diaconescu, V.; McQuarters, A. B.; Bill, E.; Dechert, S.; DeBeer, S.; Lehnert, N.; Meyer, F. Hidden non-innocence in an expanded porphyrin: Electronic structure of the siamese-twin porphyrin's dicopper complex in different oxidation states. *J. Am. Chem. Soc.* **2013**, *135*, 13892−13899.
(48) Gomes, W. C. M.; Neto, A. d. O. W.; Pimentel, P. M.; Melo, D. M. d. A.; Silva, F. R. G. e. An in situ x-ray absorption spectroscopy study of copper nanoparticles in microemulsion. *Colloids Surf., A* **2013**, *426*, 18−25.
(49) Nayak, C.; Bhattacharyya, D.; Jha, S. N.; Sahoo, N. K. In situ xas study on growth of pvp-stabilized cu nanoparticles. *ChemistrySelect* **2018**, *3*, 7370−7377.
(50) J. v. Balen, *ScanIt*, 2.05, AmsterCHEM, 2017, https://www.amsterchem.com/scanit.html.
(51) Merz, L.; Haase, W. Crystal and molecular structure and magnetic properties of tetrakis-[(2-diethylaminoethanolato)-isocyanatocopper(ii)]. *J. Chem. Soc., Dalton Trans.* **1978**, 1594−1598.
(52) Nieminen, K.; Pajunen, A. The crystal structure of {2-[(3-aminopropyl)amino]ethanolato}copper(ii) bromide tetramer trihydrate, [cu4(c5h13n2o)4]br4.3h2o. *Acta Chem. Scand.* **1978**, *32*, 493−499.
(53) Dedert, P. L.; Sorrell, T.; Marks, T. J.; Ibers, J. A. Oxygenation of [tris(2-pyridyl)amine](trifluoromethanesulfonato)copper(i) in nonaqueous solvents. Synthesis and structural characterization of the cubane-like cluster [cu4(oh)4(so3cf3)2[n(c5h4n)3]4][so3cf3]-2.C3h6o. *Inorg. Chem.* **1982**, *21*, 3506−3517.
(54) Ackermann, J.; Meyer, F.; Pritzkow, H. Unusual oligonuclear copper(ii) complexes based on a bis(tridentate) compartmental pyrazolate ligand. *Z. Anorg. Allg. Chem.* **2004**, *630*, 2627−2631.
(55) Eberhardt, J. K.; Glaser, T.; Hoffmann, R.-D.; Fröhlich, R.; Würthwein, E.-U. A tetranuclear hydroxo-bridged copper(ii) complex with primaryn-acylamidines as ligands: Preparation, structural, and magnetic characterisation. *Eur. J. Inorg. Chem.* **2005**, *2005*, 1175−1181.
(56) Lopez, N.; Vos, T. E.; Arif, A. M.; Shum, W. W.; Noveron, J. C.; Miller, J. S. Structure and magnetic properties of a hydroxo-bridged copper(ii) distorted cubane stabilized via supramolecular hydrogen bonding with an ionic hexafluoroacetylacetonate. *Inorg. Chem.* **2006**, *45*, 4325−4327.
(57) Bowmaker, G. A.; Di Nicola, C.; Marchetti, F.; Pettinari, C.; Skelton, B. W.; Somers, N.; White, A. H. Synthesis, spectroscopic and structural characterization of some novel adducts of copper(ii) salts with unidentate nitrogen bases. *Inorg. Chim. Acta* **2011**, *375*, 31−40.
(58) Zhang, X.; Li, B.; Zhang, J. An efficient strategy for self-assembly of DNA-mimic homochiral 1d helical cu(ii) chain from achiral flexible ligand by spontaneous resolution. *Inorg. Chem.* **2016**, *55*, 3378−3383.
(59) Rana, S.; Prasoon, A.; Sadhukhan, P.; Jha, P. K.; Sathe, V.; Barman, S. R.; Ballav, N. Spontaneous reduction of copper(ii) to copper(i) at solid−liquid interface. *J. Phys. Chem. Lett.* **2018**, *9*, 6364−6371.
(60) Fry, H. C.; Scaltrito, D. V.; Karlin, K. D.; Meyer, G. J. The rate of o2 and co binding to a copper complex, determined by a "flash-and-trap" technique, exceeds that for hemes. *J. Am. Chem. Soc.* **2003**, *125*, 11866−11871.

DOI: 10.1021/acs.inorgchem.9b01921
Inorg. Chem. 2019, 58, 13007−13019